On the interaction of wind and extreme gravity waves due to modulational instability

J. Touboul and C. Kharif
Institut de Recherche sur les Phénomènes Hors Equilibre, Technopôle de Château-Gombert, 49 rue Joliot Curie, B.P. 146, 13384 Marseille Cedex 13, France

(Received 9 August 2006; accepted 28 September 2006; published online 30 October 2006)

Freak waves are generated numerically by means of modulational instability. Their interaction with wind is investigated. Wind is modeled as Jeffreys' sheltering mechanism. Contrary to the case without wind, it is found that wind sustains the maximum of modulation due to the Benjamin-Feir instability. The general kinematic behavior observed for freak waves due to dispersive focusing is recovered here, even if the underlying physics are different in both cases. © *2006 American Institute of Physics*. [DOI: 10.1063/1.2374845]

Extreme wave events such as rogue waves correspond to large-amplitude waves occurring suddenly on the sea surface. *In situ* observations provided by oil and shipping industries and capsizing of giant vessels confirm the existence of such events. Up to now there is no definitive consensus about a unique definition of a rogue wave event. The definition based on height criterion is often used. When the height of the wave exceeds twice the significant height it is considered as a rogue wave. Owing to the non-Gaussian and nonstationary character of the water wave fields on the sea surface, it is a very tricky task to compute the probability density function of rogue waves. So, the approaches presented herein are rather deterministic than statistical. Recently, Refs. 1 and 2 provided reviews on the physics of these events when the direct effect of the wind is not considered. Rogue waves can occur far away from storm areas where wave fields are generated. In that case huge waves are possible on quasi-still water.

There are a number of physical mechanisms producing the occurrence of rogue waves. Extreme wave events can be due to refraction (presence of variable currents or bottom topography), dispersion (frequency modulation), wave instability (Benjamin-Feir instability), soliton interactions, etc. that may focus the wave energy into a small area. All these different mechanisms can work without direct effect of wind on waves. More details can be found in Refs. 2 and 3.

Among the mechanisms that generate extreme wave events, is the modulational instability or the Benjamin-Feir instability. Numerical simulations of the fully nonlinear equations have been performed by Refs. 4–6. Due to a resonant four wave interaction, the uniform wave trains suffer modulation-demodulation cycles (the Fermi-Pasta-Ulam recurrence). At the maximum of modulation a frequency downshift is observed and very steep waves occur.

Several experimental and theoretical studies have concerned the wind action on the modulational instability.[7–10] Herein we used a different theory based on the Jeffreys sheltering mechanism to describe the air flow separation over very steep waves.

Recently, the authors in Ref. 11 took interest in the interaction of wind and freak waves due to dispersive focusing. They found a weak amplification of the freak waves under the action of wind, and a significant increase of their lifetime. Those observations were explained by means of Jeffreys' sheltering mechanism. The purpose of this Brief Communication is to extend those results to freak waves due to modulational instability.

The fluid is assumed to be inviscid and the motion irrotational, such that the velocity $\mathbf{u}$ may be expressed as the gradient of a potential $\phi(x,z,t):\mathbf{u}=\nabla\phi$. If the fluid is assumed to be incompressible, the equation that holds throughout the fluid is the Laplace's equation.

The waves are supposed to propagate in infinite depth, and the bottom condition writes

$$\nabla\phi \rightarrow 0 \quad \text{when } z \rightarrow -\infty. \tag{1}$$

The kinematic requirement that a particle on the sea surface, $z=\eta(x,t)$, remains on it is expressed by

$$\frac{\partial\eta}{\partial t}+\frac{\partial\phi}{\partial x}\frac{\partial\eta}{\partial x}-\frac{\partial\phi}{\partial z}=0 \quad \text{on } z=\eta(x,t). \tag{2}$$

Since surface tension effects are ignored, the dynamic boundary condition which corresponds to pressure continuity through the interface, can be written

$$\frac{\partial\phi}{\partial t}+\frac{(\nabla\phi)^2}{2}+g\eta+\frac{p_a}{\rho_w}=0 \quad \text{on } z=\eta(x,t), \tag{3}$$

where g is the gravitational acceleration, p_a is the pressure at the sea surface, and ρ_w is the density of water. The atmospheric pressure at the sea surface can vary in space and time.

By introducing the potential velocity at the free surface $\phi^s(x,t)=\phi(x,\eta(x,t),t)$, Eqs. (2) and (3) write

$$\frac{\partial\phi^s}{\partial t}=-\eta-\frac{(\nabla\phi^s)^2}{2}+\frac{1}{2}W^2[1+(\nabla\eta)^2]-p_a, \tag{4}$$

$$\frac{\partial\eta}{\partial t}=-\nabla\phi^s\cdot\nabla\eta+W[1+(\nabla\eta)^2], \tag{5}$$

where

$$W = \frac{\partial \phi}{\partial z}(x, \eta(x,t), t). \tag{6}$$

Equations (4) and (5) are given in dimensionless form. Reference length, reference velocity and reference pressure are $1/k_0$, $\sqrt{g/k_0}$, and $\rho_w g/k_0$ respectively.

The numerical method used to solve the evolution equations is based on a pseudo-spectral treatment with a fourth-order Runge-Kutta integrator with constant time step, similar to the method developed by Ref. 12. More details can be found in Ref. 13.

It is well known that the uniformly traveling wave train of the Stokes' waves are unstable to the Benjamin-Feir instability, or modulational instability, which results from a quartet resonance, that is, a resonance interaction between four components of the wave field. This instability corresponds to a quartet interaction between the fundamental component k_0 counted twice and two satellites $k_1 = k_0(1+p)$ and $k_2 = k_0(1-p)$ where p is the wave number of the modulation. Instability occurs when the following resonance conditions are fulfilled:

$$k_1 + k_2 = 2k_0, \tag{7}$$

$$\omega_1 + \omega_2 = 2\omega_0, \tag{8}$$

where ω_i with $i=0,1,2$ are frequencies of the carrier and satellites. A presentation of the different classes of instability of the Stokes waves is given in the review paper by Dias and Kharif.[14]

The procedure used to calculate the linear stability of the Stokes waves is similar to the method described by Kharif and Ramamonjiarisoa.[15] Let $\eta = \bar{\eta} + \eta'$ and $\phi = \bar{\phi} + \phi'$ be the perturbed elevation and perturbed velocity potential where $(\bar{\eta}, \bar{\phi})$ and (η', ϕ') correspond, respectively, to the unperturbed Stokes wave and infinitesimal perturbative motion $(\eta' \ll \bar{\eta}, \phi' \ll \bar{\phi})$. Following Ref. 16, the Stokes wave of amplitude a_0 and wave number k_0 is computed iteratively. This decomposition is introduced in the boundary conditions (4) and (5) linearized about the unperturbed motion, and the following form is used:

$$\eta' = \exp(\lambda t + ipx) \sum_{-\infty}^{\infty} a_j \exp(ijx), \tag{9}$$

$$\phi' = \exp(\lambda t + ipx) \sum_{-\infty}^{\infty} b_j \exp(ijx + \gamma_j z), \tag{10}$$

where λ, a_j, and b_j are complex numbers and where $\gamma_j = |p + j|$. An eigenvalue problem for λ with eigenvector $\mathbf{u} = (\mathbf{a_j}, \mathbf{b_j})^{\mathbf{t}} : (\mathbf{A} - \lambda \mathbf{B})\mathbf{u} = 0$ is obtained, where $\mathbf{A}$ and $\mathbf{B}$ are complex matrices depending on the unperturbed wave steepness of the basic wave. The physical disturbances are obtained from the real part of the complex expressions η' and ϕ' at $t=0$.

References 17 and 18 showed that the dominant instability of a uniformly traveling train of Stokes' waves in deep water is the two-dimensional modulational instability, or class I instability, as soon as its steepness is less than $\epsilon = 0.30$.

In our simulations, the initial condition is a Stokes wave of steepness $\epsilon = 0.11$, disturbed by its most unstable perturbation which corresponds to $p \approx 0.20 = 1/5$. The fundamental wave number of the Stokes wave is $k_0 = 5$ and the dominant sidebands are $k=4$ and $k=6$ for the subharmonic and superharmonic part of the perturbation, respectively. There exists higher harmonics present in the interactions which are not presented here. The normalized amplitude of the perturbation relative to Stokes wave amplitude is initially taken to be equal to 10^{-3}. The order of nonlinearity is $M=6$, and the number of mesh points is $N > (M+1)k_{\max}$, where $k_{\max}$ is the highest harmonic taken into account in the simulation. The latter criterion concerning N is introduced to avoid aliasing errors. To compute the long time evolution of the wave packet the time step Δt is chosen to be equal to $T/100$, where T is the fundamental period of the basic wave. This temporal discretization satisfies the CFL condition.

Previous works on the rogue wave have not considered the direct effect of wind on their dynamics. It was assumed that they occur independently of wind action, that is far away from storm areas where wind wave fields are formed. Herein the Jeffreys' theory (see Ref. 19) is invoked for the modelling of the pressure, p_a. Jeffreys suggested that the energy transfer was due to the form drag associated with the flow separation occurring on the leeward side of the crests. The air flow separation would cause a pressure asymmetry with respect to the wave crest resulting in a wave growth. This mechanism can be invoked only if the waves are sufficiently steep to produce air flow separation. Reference 20 has shown that separation occurs over near breaking waves. For weak or moderate steepness of the waves this phenomenon cannot apply and the Jeffreys' sheltering mechanism becomes irrelevant.

Following Ref. 19 the pressure at the interface $z = \eta(x,t)$ is related to the local wave slope according to the following expression:

$$p_a = \rho_a s (U - c)^2 \frac{\partial \eta}{\partial x}, \tag{11}$$

where the constant, s is termed the sheltering coefficient, U is the wind speed, c is the wave phase velocity, and ρ_a is the atmospheric density. The sheltering coefficient, $s=0.5$, has been calculated from the experimental data. In order to apply the relation (11) for only very steep waves we introduce a threshold value for the slope $(\partial \eta / \partial x)_c$. When the local slope of the waves becomes larger than this critical value, the pressure is given by Eq. (11), otherwise the pressure at the interface is taken to be equal to a constant which is chosen to be equal to zero without loss of generality. This means that wind forcing is applied locally in time and space.

The initial condition described previously is propagated numerically with the high order spectral method. Both cases with and without wind are studied and compared.

For the case without wind, the time histories of the normalized amplitude of the carrier, lower sideband and upper

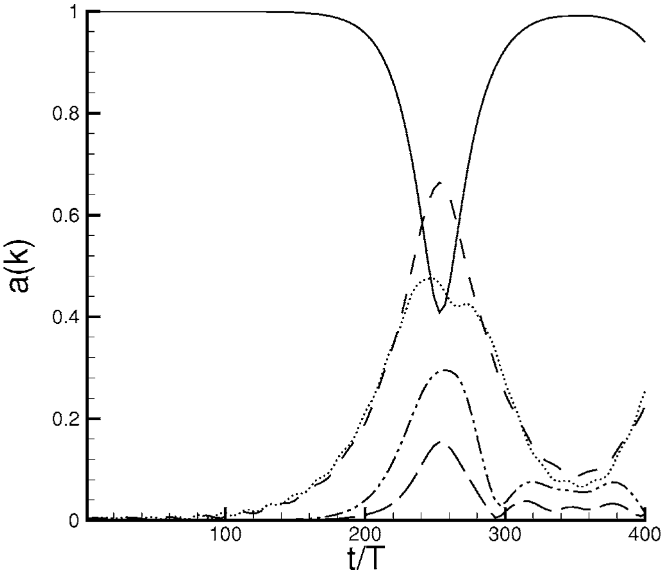

FIG. 1. Time histories of the amplitude of the fundamental, $k_0=5$ (solid line), subharmonic, $k_1=4$ (dashed line), and superharmonic, $k_2=6$ (dotted line), modes without wind action. The two lowest curves (dashed-dotted lines) correspond to the modes $k_3=3$ and $k_4=7$.

sideband of the most unstable perturbation are plotted in Fig. 1. Another perturbation which was initially linearly stable becomes unstable in the vicinity of maximum of modulation resulting in the growth of the sidebands $k_3=3$ and $k_4=7$. The nonlinear evolution of the two-dimensional wave train exhibits the Fermi-Pasta-Ulam recurrence phenomenon. This phenomenon is characterized by a series of modulation-demodulation cycles in which initially uniform wave trains become modulated and then demodulated until they are again uniform. Herein one cycle is reported. At $t \approx 360$ T the initial condition is more or less recovered. At the maximum of modulation $t=260$ T, one can observe a temporary frequency (and wave number) downshifting since the subharmonic mode $k_1=4$ is dominant. At this stage a very steep wave occurs in the group.

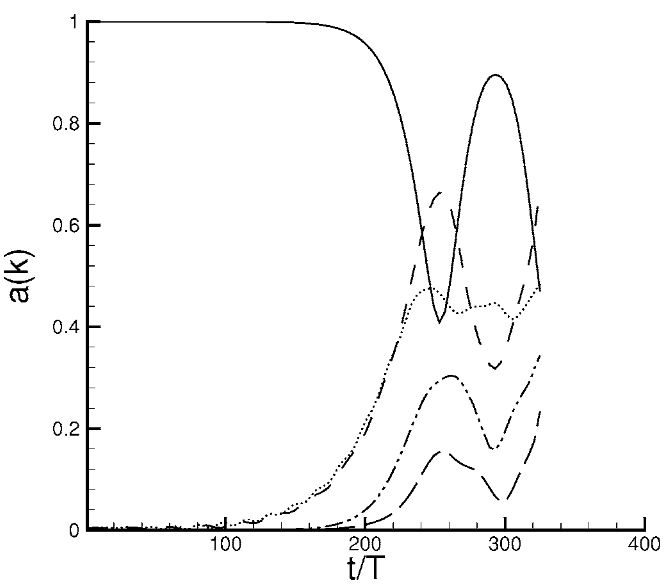

FIG. 2. Time histories of the amplitude of the fundamental, $k_0=5$ (solid line), subharmonic, $k_1=4$ (dashed line), and superharmonic, $k_2=6$ (dotted line), modes with wind action ($U=1.75c$). The two lowest curves (dashed-dotted lines) correspond to the modes $k_3=3$ and $k_4=7$.

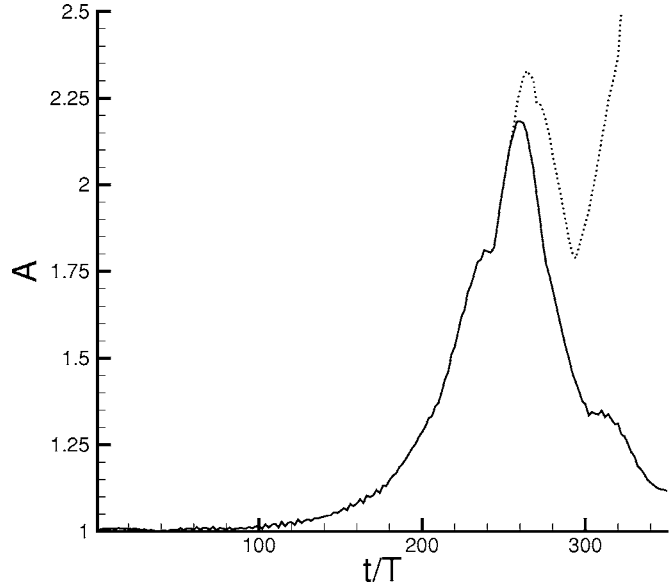

FIG. 3. Numerical maximum elevation normalized by the initial wave amplitude (amplification factor) as a function of time without wind (solid line) and with wind (dotted line) for $U=1.75c$.

Figure 2 is similar to Fig. 1, except that now water waves evolve under wind action. Wind forcing is applied over crests of slopes larger than $(\partial\eta/\partial x)_c=0.405$. This condition is satisfied for 256 T $<t<$ 270 T, that is during the maximum of modulation which corresponds to the formation of the extreme wave event. When the values of the wind velocity are too high numerical simulations fail during the formation of the rogue wave event, due to breaking. During the breaking wave process the slope of the surface becomes infinite, leading numerically to a spread of energy into high

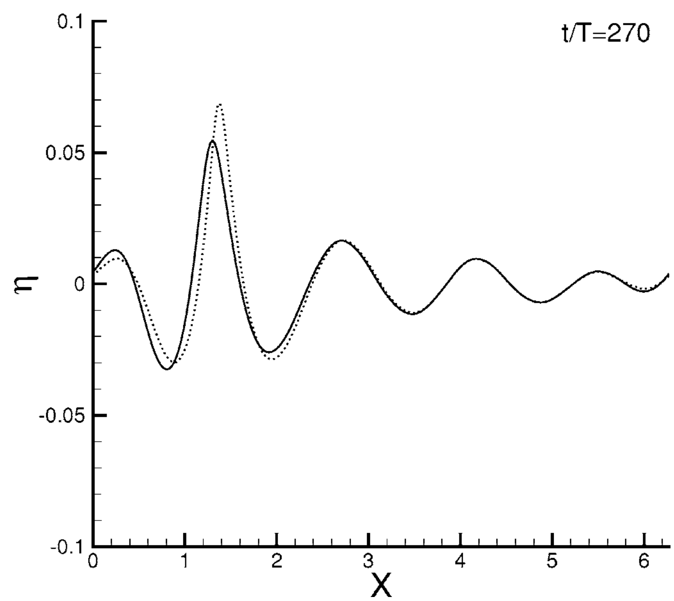

FIG. 4. Surface wave profile at $t=270T$: without wind (solid line) and with wind (dotted line).

wave numbers. This local steepening is characterized by a numerical blowup. In order to avoid a too early breaking wave, the wind velocity is fixed at $U \approx 1.75c$. Owing to the weak effect of the wind on the phase velocity of the crests on which it acts, the phase velocity is computed without wind. The effect of the wind reduces significantly the demodulation cycle and thus sustains the rogue wave event. This feature is clearly shown in Fig. 3. The amplification factor A is the maximal wave height of the packet normalized by the initial wave height of the Stokes wave. It is stronger in the presence of wind and the rogue wave criterion $A > 2$ is satisfied during a longer period of time. Figure 4 displays the water wave profile at $t = 170$ T in the vicinity of the maximum of modulation with and without wind. The solid line corresponds to waves propagating without wind while the dotted line represents the wave profile under wind action. This figure shows that the wind does not significantly modify the phase velocity of the very steep waves while it increases their height.

To summarize the results, it appears that extreme wave events generated by modulational instability in the presence of wind behaves similarly to those due to dispersive spatio-temporal focusing discussed in Ref. 11 at least from a kinematic point of view. An amplification of the freak wave event and a significant increase of its lifetime are found. The behavior observed here is correlated with the change in the Fermi-Pasta-Ulam recurrence.

[1] K. B. Dysthe, "Modelling a 'rogue wave'—Speculations or a realistic possibility?" in *Rogues Waves 2000*, edited by M. Olagnon and G. A. Athanassoulis (Brest, France, 2001), pp. 255–264.
[2] C. Kharif and E. Pelinovsky, "Physical mechanisms of the rogue wave phenomenon," Eur. J. Mech. B/Fluids **22**, 603 (2003).
[3] C. Kharif and E. Pelinovsky, *Freak Waves Phenomenon: Physical Mechanisms and Modelling*, edited by J. Grue and K. Trulsen (Springer-Verlag, Berlin, 2006), pp. 107–172.
[4] K. L. Henderson, D. H. Peregrine, and J. W. Dold, "Unsteady water wave modulations: Fully nonlinear solutions and comparison with the nonlinear Schrödinger equation," Wave Motion **29**, 341 (1999).
[5] J. B. Song and M. L. Banner, "On determining the onset and strength of breaking for deep water waves. Part 1: unforced irrotational wave groups," J. Phys. Oceanogr. **32**, 2541 (2002).
[6] A. I. Dyachenko and V. E. Zakharov, "Modulation instability of Stokes waves → freak wave," JETP Lett. **81**, 255 (2005).
[7] L. F. Bliven, "Experimental study of the influence of wind on Benjamin-Feir sideband instability," J. Fluid Mech. **162**, 237 (1986).
[8] K. Trulsen and K. B. Dysthe, "Action of wind stress and breaking on the evolution of a wave train," in *IUTAM Symposium on Breaking Waves 1991*, edited by M. L. Banner and R. H. J. Grimshaw (Springer-Verlag, Berlin, 1992), pp. 243–249.
[9] M. I. Banner and X. Tian, "On the determination of the onset of breaking for modulating surface gravity water waves," J. Fluid Mech. **367**, 107 (1998).
[10] M. I. Banner and J. Song, "On determining the onset and strength of breaking for deep water waves. Part II: Influence of wind forcing and surface shear," J. Phys. Oceanogr. **32**, 2559 (2002).
[11] J. Touboul, J. P. Giovanangeli, C. Kharif, and E. Pelinovsky, "Freak waves under the action of wind: Experiments and simulations," Eur. J. Mech. B/Fluids **25**, 662 (2006).
[12] D. G. Dommermuth and D. K. P. Yue, "A high-order spectral method for the study of nonlinear gravity waves," J. Fluid Mech. **184**, 267 (1987).
[13] C. Skandrani, C. Kharif, and J. Poitevin, "Nonlinear evolution of water surface waves: The frequency downshifting phenomenon," Contemp. Math. **200**, 157 (1996).
[14] F. Dias and C. Kharif, "Nonlinear gravity and capillary-gravity waves," Annu. Rev. Fluid Mech. **31**, 301 (1999).
[15] C. Kharif and A. Ramamonjiarisoa, "Deep water gravity wave instabilities at large steepness," Phys. Fluids **31**, 1286 (1988).
[16] M. S. Longuet-Higgins, "Bifurcation in gravity waves," J. Fluid Mech. **151**, 457 (1985).
[17] J. W. McLean, Y. C. Ma, D. U. Martin, P. G. Saffman, and H. C. Yuen, "Three-dimensional instability of finite-amplitude water waves," Phys. Rev. Lett. **46**, 817 (1981).
[18] J. W. McLean, "Instabilities of finite-amplitude water waves," J. Fluid Mech. **114**, 315 (1982).
[19] H. Jeffreys, "On the formation of wave by wind," J. Proc. R. Soc. N. S. W. **107**, 189 (1925).
[20] M. I. Banner and W. K. Melville, "On the separation of air flow over water waves," J. Fluid Mech. **77**, 825 (1976).